Tuning piezoresistive transduction in nanomechanical resonators by geometrical asymmetries

J. Llobet,[1] M. Sansa,[1,a)] M. Lorenzoni,[1] X. Borrisé,[2] A. San Paulo,[3] and F. Pérez-Murano[1,b)]
[1]*Institut de Microelectrònica de Barcelona (IMB-CNM CSIC), Campus UAB, 08193 Bellaterra, Spain*
[2]*Institut Català de Nanociència i Nanotecnologia (ICN2), Campus UAB, 08193 Bellaterra Spain*
[3]*Instituto de Microelectrónica de Madrid (IMM-CSIC), 28760 Tres Cantos, Madrid, Spain*

(Received 30 April 2015; accepted 3 August 2015; published online 17 August 2015)

The effect of geometrical asymmetries on the piezoresistive transduction in suspended double clamped beam nanomechanical resonators is investigated. Tapered silicon nano-beams, fabricated using a fast and flexible prototyping method, are employed to determine how the asymmetry affects the transduced piezoresistive signal for different mechanical resonant modes. This effect is attributed to the modulation of the strain in pre-strained double clamped beams, and it is confirmed by means of finite element simulations. © *2015 AIP Publishing LLC*.
[http://dx.doi.org/10.1063/1.4928709]

Resonating nanomechanical structures are attractive building blocks for the realization of high performance sensors and integrated oscillators.[1] For example, a double clamped nanometric beam (DCB) (a silicon nanowire or a carbon nanotube) presents very large resonance frequency and extremely low mass, which are both highly convenient to detect minuscule quantities of mass.[2,3] Also, DCB[4] or more complex structures[5] can be integrated within CMOS circuits to build high frequency oscillators that eventually may substitute present hybrid and heterogeneous integration approaches for signal processing.

The practical application of nanomechanical resonators requires an efficient method for detecting their oscillation, which becomes increasingly difficult as the dimensions of the structures shrink. Electrical read-out of the oscillation is one of the most straightforward ways of obtaining compact systems, enabling the possibility of simultaneous detection of a large number of resonating elements. Electrical transduction can be implemented, for example, by capacitive,[5] piezo-electric,[6] or piezo-resistive[7] read-out. Compared to other methods, piezoresistive read-out presents the advantage of easy implementation, since the beam itself acts as a piezoresistive gauge, simplifying device design and fabrication.

While the so called giant piezoresistance effect has enabled piezoresistive read-out in DCB silicon nanowires fabricated by bottom-up methods,[8,9] it has not been observed in top-down fabricated DCBs. Recently, it has been shown that geometrical asymmetries present in DCBs cause an enhancement of the piezoresistive transduction, allowing to obtain large read-out electrical signals from silicon nanowire resonators obtained by top-down and bottom-up fabrication methods.[10] Here, we show that piezo-resistive read-out signals in DCB nanomechanical resonators can be tuned by engineering the asymmetry of the device, and in particular, by inducing deliberate asymmetries that enhance the transduction of specific resonant modes.

We have focused the present study on DCB nanomechanical resonators fabricated by a fast, accurate, and flexible prototyping method based on the combination of focused ion beam (FIB) exposure and wet silicon etching,[11] which is compatible with CMOS technology.[12] Next, we present the main details of the fabrication process, the electrical characterization setup, and the experimental results that show the influence of the geometrical asymmetry on the transduced signals. The behavior is explained by means of modelling the modal mechanical response of the DCB.

DCB were fabricated by means of a prototyping method that allows for a very high geometrical control of the device dimensions.[11,13] Figure 1(a) shows the basic steps of the fabrication process. Starting substrates are dices obtained from silicon on insulator (SOI) wafers (i). The silicon device layer orientation is $\langle 110 \rangle$, the thickness is $2 \pm 0.5\,\mu$m, it is p-type doped by boron, and the resistivity is around $10\,\Omega$m. The thickness of the silicon dioxide layer is of $2\,\mu$m $\pm$ 5%. The first fabrication step consists in local gallium implantation of the SOI layer by FIB, to define the silicon nanowire, the side gate electrode (when required), and the contact pads and lines (ii). The ion dose used for the implantation is 10^{16} at$\cdot$cm^{-2} and the acceleration voltage is 30 kV. The implanted silicon volume becomes amorphous and doped with gallium for a thickness of around 35–40 nm. As a result, its physicochemical structure changes, becoming a material that better resists a silicon etching. The second step consists on a TMAH etching (25% solution at 80 °C) that removes crystalline silicon anisotropically (iii). By means of an appropriate choice of the orientation of the device with respect to the crystalline orientation of the SOI layer, the silicon nanowire is released from the substrate because of the removal of the non-exposed silicon below the nanowire, while the contact lines and pads show a good stepped profile. The last fabrication step consists in an annealing at high temperature in a boron environment in order to recrystallize the exposed silicon and to improve the electrical conductivity (iv). Typically, the final resistivity of the nanowire lies between 10^{-3} and $10^{-4}\,\Omega$m at the end of

a)Present address: CEA-LETI, rue des Martyrs, 38054 Grenoble, France.
b)Author to whom correspondence should be addressed. Electronic mail: francesc.perez@csic.es

This article is copyrighted as indicated in the article. Reuse of AIP content is subject to the terms at: http://scitation.aip.org/termsconditions. Downloaded to IP: 161.111.180.191 On: Wed, 23 Dec 2015 12:43:41

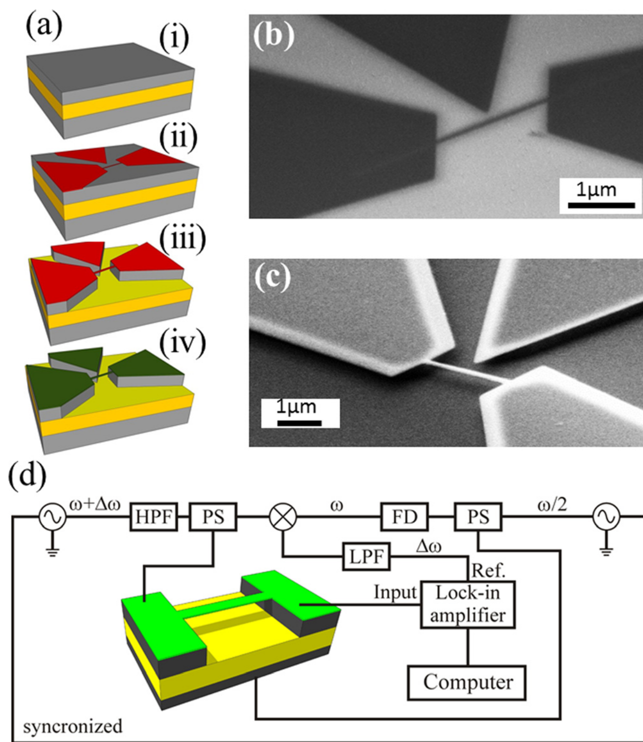

FIG. 1. (a) Steps of the fabrication process: (i) Starting substrate: SOI wafer; (ii) local gallium implantation by focused ion beam; (iii) TMAH etching to remove selectively the silicon below the non-implanted areas; (iv) annealing at high temperature in a boron environment in order to recover the crystallinity of the beam and the electrical conductivity. (b) SEM image of a device defined using the method shown in (a) after the gallium implantation. (c) SEM image of the same device at the end of the fabrication process. (d) Schematics of the electrical setup to detect the frequency response of double clamed beam. HPF: High pass filter. PS: Power splitter. LPF: Low pass filter. FD: Frequency doubler.

the fabrication. The dices are wire bonded to a PCB board, by directly bonding electrical wires to the silicon pads. The process does not include any metallization step.

Figures 1(b) and 1(c) show an example of a device fabricated using this method. The images show a double clamped, free standing nano-beam with a side gate electrode close to it. The side gate electrode can be used to exert an electrostatic force to induce the in-plane oscillation of the beam. However, in all the experiments reported here, we have used back-gate actuation to force the out-of-plane vibration of the beam. Figure 1(b) is a SEM image after the FIB exposure, and Figure 1(c) is an image at the end of the fabrication process. As each device is exposed individually, their dimensions can be customized, facilitating the experimentation of varied beam geometries.

The measurements of the DCB resonators have been performed in a vacuum chamber at a pressure of 10^{-6} mbar and at room temperature. The electromechanical characterization is performed by means of a frequency down-mixing method, taking advantage of the non-linear dependence of the piezoresistance change with the actuation voltage. The motion of the resonator generates a high frequency signal, which is down-mixed (i.e., translated to lower frequencies) at the device level by non-linear mixing with the signal applied through the beam. The low frequency component of the mixing carries information about the oscillation amplitude of the nanowire. In all the devices presented here, the actuation is performed electrostatically through the silicon substrate (back gate configuration).

In the previous works, frequency down-mixing has been implemented in DCB resonators using different setups: Frequency Modulation (FM),[14,15] 2 sources 1ω,[16] and 2 sources 2 ω.[17] The first two methods require that the modulation of the beam conductivity occurs at the same frequency than the beam oscillation frequency, while the third method requires that the modulation takes place at the double of the oscillation frequency. As we have demonstrated before,[15] the asymmetry-induced transduction enhancement in top-down fabricated DCB generates transduced signals at the same frequency than the oscillation frequency. Taking this into account, we have implemented a variation of the 2 sources 1 ω technique, which minimizes the parasitic capacitance coupling between the gate electrode and the device, as displayed in Figure 1(d). The signal applied to the source electrode of the device is at high frequency (ω) with a typical amplitude of 200 mV, while the signal applied to the back-gate electrode has a frequency of $\omega/2+\Delta\omega$ and an amplitude of 1.25 V, being the value of $\Delta\omega$ typically of 2 kHz. In this way, the electrostatic force to actuate the device has a frequency of $\omega+\Delta\omega$, and, consequently, the mixing takes place between signals with frequency close to ω. The current that circulates through the beam is measured at the drain electrode by a lock in amplifier at the frequency $2\cdot\Delta\omega$.

To study the effects of the asymmetry in the electromechanical transduction, tapered double clamped silicon beams have been designed and fabricated. Figures 2(a) and 2(d) show two SEM images of this kind of devices. The length of the beams is 4.2 μm for both devices. The device in Figure 2(a) is symmetric, while the device in Figure 2(d) presents a tapering factor (α) of 2.3, where $\alpha = w_1/w_2$ is defined as the relation between the widths at the two clamping edges of the beam, w_1 and w_2.

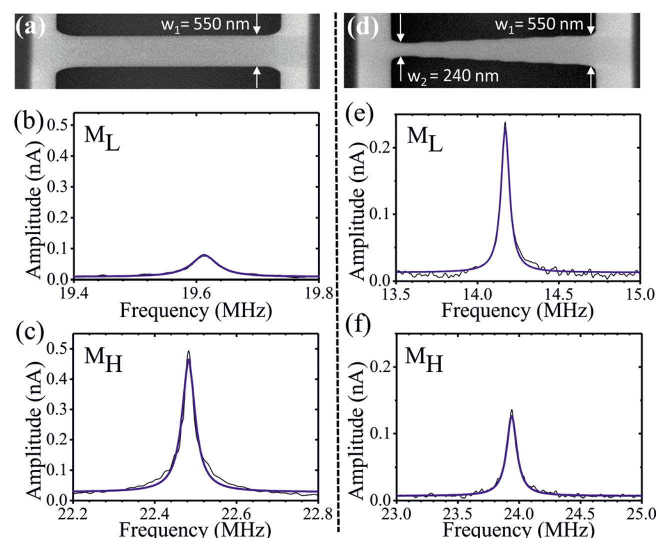

FIG. 2. (a) SEM image of a symmetric double clamped beam. (b) and (c) Electrical signals obtained from the device shown in (a) using the setup described in Figure 1(d). M_L stands for mode of lower frequency and M_H stands for mode of higher frequency. (d) SEM image of an asymmetric double clamped beam. (e) and (f) Electrical signals obtained from the device shown in (d) using the setup described in Figure 1(d). Black curves are the experimental data and blue curves are the Lorentzian fitting of the curve.

This article is copyrighted as indicated in the article. Reuse of AIP content is subject to the terms at: http://scitation.aip.org/termsconditions. Downloaded to IP: 161.111.180.191 On: Wed, 23 Dec 2015 12:43:41

The frequency response of both devices is shown in Figures 2(b) and 2(c) and Figures 2(e) and 2(f) for the two modes of lower frequency. All the measurements presented in this work are the result of a frequency sweep from 10 to 40 MHz. The figures show two resonance peaks between 12 and 30 MHz for both devices. We name the resonant modes as M_L (lower resonance frequency mode) and M_H (higher resonance frequency mode). For the symmetric device ($\alpha = 1$), the current amplitude of the M_H mode, I_H, is larger than the current amplitude of the M_L mode, I_L. On the contrary, for the tapered device ($\alpha = 2.3$), the current amplitude of M_L is larger than the current amplitude of M_H. The ratio between the current amplitude of mode M_L divided by the current amplitude of mode M_H is defined as $\gamma = I_L/I_H$.

We have characterized the frequency response for a group of similar devices with diverse values of the tapering factor α.[18] Figures 3(a) and 3(b) represent, for all the devices, the experimental values of the current signal as a function of the tapering factor (α). It is found that the current signal increases with the tapering factor (α) for the mode M_L, while it decreases for the mode M_H. The data in Figures 3(a) and 3(b) show a certain dispersion, which is due to the fact that they correspond to devices obtained in different fabrication batches (for example, a variation in the final thicknesses in the range ± 5 nm may occur from fluctuations in the ion current from one exposure to another) and to the fact that the range of dimensions of the devices is different: as it is shown in Ref. 18, the devices with the largest tapering factors are also wider, due to fabrication constraints. To overcome the effect of this dispersion, we have represented in Figure 3(c) the amplitude ratio $\gamma = I_L/I_H$, which is obtained for each device independently. The solid line is drawn to better show the tendency of γ to increase as a function of α.

Next, we show that the dependence on the tapered beam asymmetry of the electrical signals presented in Figures 2 and 3 is linked to the same physical mechanism responsible

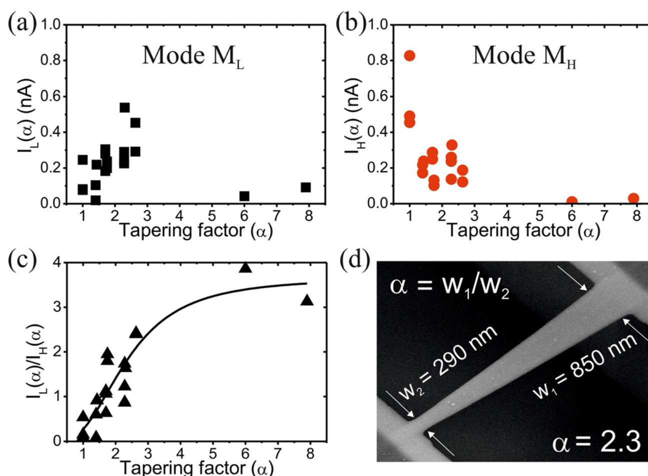

FIG. 3. Experimental values of the transduced signal as a function of the tapering factor (α) for a set of 19 devices: (a) detected current I_L for the resonant mode of lower frequency (M_L); (b) detected current I_H for the resonant mode of higher frequency (M_H); (c) experimental values of the amplitude ratio (γ) defined as I_L/I_H. The ratio is obtained for each device separately. The solid line is drawn to better show the tendency. (d) SEM image of one of the devices with $\alpha = 2.3$.

for the enhancement of the linear piezoresistive transduction described previously.[10]

The influence of the geometrical asymmetry of the devices on the electromechanical transduction is analyzed taking into account the model developed previously.[10] The onset of the linearized piezoresistive transduction occurs when the DCB is in a pre-strained situation in equilibrium, and then its longitudinal strain is modulated around this equilibrium position. This pre-strain situation happens as a consequence of an asymmetric beam profile at rest. As it is demonstrated previously,[10] the larger the value of the pre-strain, the larger will be the piezoresistive transduced signal. This effect is more relevant in NEMS structure rather than in MEMS structure because the relative value of the pre-strain with respect to the strain induced during the oscillation is larger in small, ultra-thin beams. To calculate the value of the strain modulation, the values of the pre-strain of the structure and of the additional longitudinal strain induced by the oscillation of the nanowire have to be determined. In addition, since each resonant mode has a specific modal shape, they will contribute differently to the strain modulation.

In general, the beam profile $w(x,t)$, defined as the out-of-plane displacement with respect to a perfectly straight beam, can be written as

$$w(x,t) = d_0\phi_0(x) + a_n(\omega)\phi_n(x)\cos(\omega t), \tag{1}$$

where x is the longitudinal coordinate along the beam, ω is the driving frequency, $\phi_0(x)$ is the asymmetric beam profile at rest normalized to the maximum deflection at rest d_0, and $\phi_n(x)$ is the nth vibration mode profile normalized to the maximum vibration amplitude of the mode $a_n(\omega)$.

The oscillation of the nanowire, induced by the electrostatic force originated from the back-gate electrode, causes a modulation of the strain, which is responsible for the piezoresistive transduction, i.e., a time-dependent variation of the beam resistance. The corresponding change of resistance $\Delta R(t)$ is given by[10]

$$\frac{\Delta R(t)}{R_u} = \frac{Ga_n(\omega)d_0}{L}\cos(\omega t)\int_0^L \phi_0'(x)\phi_n'(x)dx + \frac{Ga_n^2(\omega)}{4L}\cos(2\omega t)\int_0^L \phi_n'^2(x)dx, \tag{2}$$

where G is the piezoresistive gauge factor, R_u is the undeflected beam resistance, L is the length of the beam, and $\phi_0'(x)$ and $\phi_n'(x)$ are the spatial derivatives of the beam profile at rest and of the nth mode profile, respectively. As the electrical read-out method employed in this work only detects the electrical transduction that occurs at the oscillation frequency, we are only interested in the first summand of the second term in Eq. (2). Also, we assume that the measured signal of the lock-in amplifier, I_n, is proportional to $\Delta R(t)$

$$I_n \cong G\frac{1}{2L}\frac{V_0}{R_u}a_n d_0\int_0^L \phi_0'(x)\phi_n'(x)dx = G\frac{V_0}{R_u}a_n d_0 p_n, \tag{3}$$

where V_0 is the amplitude of the signal applied to the source electrode of the device. The factor P_n is defined as

This article is copyrighted as indicated in the article. Reuse of AIP content is subject to the terms at: http://scitation.aip.org/termsconditions. Downloaded to IP: 161.111.180.191 On: Wed, 23 Dec 2015 12:43:41

$$p_n = \frac{1}{2L}\int_0^L \phi_0'(x)\phi_n'(x)dx, \quad (4)$$

and it is the factor that incorporates the presence of asymmetries in the beam.

We define the transduction as the relation between the measured electrical signal I_n and the amplitude of oscillation of the beam a_n

$$T_n(\alpha) = \frac{I_n(\alpha)}{a_n(\alpha)} \cong G\frac{V_0}{R_u(\alpha)}d_0 p_n(\alpha). \quad (5)$$

In Eq. (5), it has been made explicit which factors depend on the tapering asymmetry α.

We have experimentally determined the beam profile by atomic force microscopy.[18] As a consequence of the fabrication process, the beams present a vertical deflection d_0 with a maximum displacement of around 60–70 nm. The origin of the deflection is attributed to the change of the structure of the silicon nanowires from crystalline to amorphous, as a consequence of the FIB implantation process, and the ulterior annealing that gives place to a nanocrystalline structure, as revealed from high resolution TEM characterization.[11] As a consequence, a built-in stress is induced during the process, which partially converts to additional strain at the end of the fabrication. For the symmetric devices, the maximum of the vertical deflection occurs at the center of the beam, while for asymmetric devices the maximum is displaced towards the narrower side of the beam. We have not appreciated a significant dependence of the absolute value of d_0 on the tapering factor α.

To determine the mode profiles and their derivatives, $\phi_n(x)$ and $\phi_n'(x)$, we have performed finite element simulations. We have modelled the beams with the actual geometry (dimensions, tapering factors, and deflection profiles at rest) and with an additional compressive stress to account for the experimental measured values of the resonance frequency of each mode. The finite element simulations unveil that, for symmetric devices, the M_L mode develops from the second order flexural mode in non-strained, straight double clamped beams, while the M_H mode comes from the fundamental flexural mode. The fact that the mode with a shape profile similar to the second mode is of lower frequency is caused by the high initial pre-strain in the structure, as corroborated by additional finite element simulations.[18]

The derivatives of the mode profiles obtained from the simulations have been determined numerically, and then the integration defined by Eq. (4), $P_n(\alpha)$, has been performed. Figures 4(a) and 4(b) show the asymmetry dependence of $P_n(\alpha)$ and $P_n(\alpha)/R_u(\alpha)$, respectively. According to Eq. (5), $P_n(\alpha)/R_u(\alpha)$ determines the transduction efficiency. It is observed that the effect of the asymmetry in the transduction is already highly relevant for small values of the tapering factor, especially for the mode M_L, for which the presence of tapering is necessary for obtaining a linear piezoresistive transduced signal. Finally, as it can be observed in Figure 4(c), the transduction ratio between the two modes, $T_L(\alpha)/T_H(\alpha) = P_L(\alpha)/P_H(\alpha)$, follows the experimental tendency depicted in Figure 3(c), corroborating that the main effect of the geometrical asymmetry of the device is on the piezoresistive transduction. In Ref. 18, the effect of the asymmetries in the transduction efficiency is graphically shown.

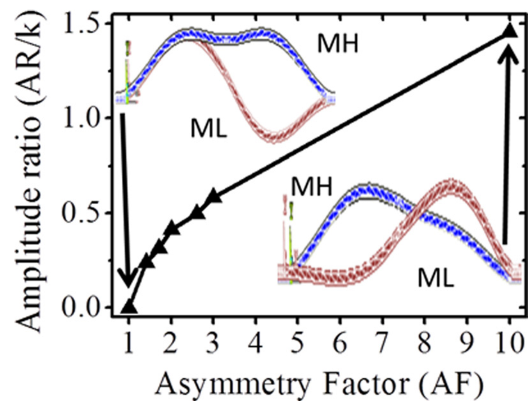

FIG. 4. Dependence of (a) $2L \cdot p_n = \int_0^L \phi_0'(x)\phi_n'(x)dx$ and (b) $P_n(\alpha)/\underline{R}_u(\alpha)$, on the tapering factor α, where $\underline{R}_u(\alpha)$ is the static resistance of the beam normalized to the resistance of the non-tapered beam. The dependencies are obtained for silicon nano-beams with similar geometries as the ones in Figure 3, and they are calculated from the determination of the beam and mode profile obtained from ANSYS simulation. (c) Dependence of $P_L(\alpha)/P_H(\alpha)$, which reflects the relation between the transduction efficiently between modes M_L and M_H according to Eq. (5). The insets of Figure 4 show the profiles for the low and high modes of beams with tapering factors of 1 and 10. They are obtained from ANSYS simulations. The points in the figures correspond to the specific values of the tapering factor that have been used in the simulations. The solid lines are drawn to better show the tendencies.

In summary, we have shown that the amplitude of the piezoresistive transduced signal generated by the mechanical oscillation of double clamped beams is highly influenced by the presence of stress and asymmetries. By properly tuning the geometrical asymmetry of the beam, the electrical signal corresponding to specific resonant modes can be enhanced or diminished. This effect can be used to design devices based on nanomechanical resonators that exploit parametric amplification or nanomechanical mass sensors with spatial discrimination of absorbing sites,[19] and it is expected to be of critical importance for enabling the electrical detection of the vibration of very thin and narrow beams fabricated by top-down methods, where pre-existing strain and stress are significantly high.

The research leading to these results received funding from the European Union's Seventh Framework Programme FP7/2007-2013, under Grant Agreement No. 318804 (SNM). Support is also acknowledged from project Force for future (CSD2010-00024).

[1] L. Nicu, V. Auzelyte, L. G. Villanueva, N. Barniol, F. Perez-Murano, W. J. Venstra, H. S. J. van der Zant, G. Abadal, V. Savu, and J. Brugger, "Nanoelectromechanical systems," in *Resonant MEMS: Fundamentals, Implementation, and Application*, edited by O. Brandt *et al*. (Wiley, 2015), pp. 287-304.
[2] J. Chaste, A. Eichler, J. Moser, G. Ceballos, R. Rurali, and A. Bachtold, Nat. Nanotechnol. 7, 301 (2012).
[3] M. S. Hanay, S. Kelber, A. K. Naik, D. Chi, S. Hentz, E. C. Bullard, E. Colinet, L. Duraffourg, and M. L. Roukes, Nat. Nanotechnol. 7, 602 (2012).
[4] J. L. Muñoz-Gamara, P. Alcaine, E. Marigó, J. Giner, A. Uranga, J. Esteve, and N. Barniol, Microelectron. Eng. 110, 246 (2013).
[5] G. Abadal, Z. J. Davis, B. Helbo, X. Borrisé, R. Ruiz, A. Boisen, F. Campabadal, J. Esteve, E. Figueras, F. Pérez-Murano, and N. Barniol, Nanotechnology 12, 100–104 (2001).

This article is copyrighted as indicated in the article. Reuse of AIP content is subject to the terms at: http://scitation.aip.org/termsconditions. Downloaded to IP: 161.111.180.191 On: Wed, 23 Dec 2015 12:43:41

[6]L. Guillermo Villanueva, R. B. Karabalin, M. H. Matheny, E. Kenig, M. C. Cross, and M. L. Roukes, Nano Lett. **11**, 5054 (2011).
[7]M. Li, H. X. Tang, and M. L. Roukes, Nat. Nanotechnol. **2**, 114 (2007).
[8]R. He and P. Yang, Nat. Nanotechnol. **1**, 42 (2006).
[9]K. Winkler, E. Bertagnolli, and A. Lugstein, Nano Lett. **15**, 1780 (2015).
[10]M. Sansa, M. Fernández-Regúlez, J. Llobet, Á. San Paulo, and F. Pérez-Murano, Nat. Commun. **5**, 4313 (2014).
[11]J. Llobet, M. Sansa, M. Gerbolés, N. Mestres, J. Arbiol, X. Borrisé, and F. Pérez-Murano, Nanotechnology **25**, 135302 (2014).
[12]G. Rius, J. Llobet, J. Arcamone, X. Borrisé, and F. Pérez-Murano, Microelectron. Eng. **86**, 1046 (2009).
[13]J. Llobet, M. Gerbolés, M. Sansa, J. Bausells, X. Borrisé, and F. Pérez-Murano, J. Micro/Nanolithogr. MEMS MOEMS **14**, 031207 (2015).
[14]V. Gouttenoire, T. Barois, S. Perisanu, J.-L. Leclercq, S. T. Purcell, P. Vincent, and A. Ayary, Small **6**, 1060 (2010).
[15]M. Sansa, M. Fernández-Regúlez, Á. San Paulo, and F. Pérez-Murano, Appl. Phys. Lett. **101**, 243115 (2012).
[16]V. Sazonova, Y. Yalsh, H. Üstünel, D. Roundy, T. A. Arlas, and P. L. McEuen, Nature **431**, 284 (2004).
[17]R. He, X. L. Feng, M. K. Roukes, and P. Yang, Nano Lett. **8**, 1756 (2008).
[18]See supplementary material at http://dx.doi.org/10.1063/1.4928709 for detailed information about the devices characterized, AFM characterization of the beams, simulation, and modelling.
[19]M. S. Hanay, S. I. Kelber, C. D. O'Connel, P. Mulvaney, J. E. Sader, and M. L. Roukes, Nat. Nanotechnol. **10**, 339–344 (2015).

This article is copyrighted as indicated in the article. Reuse of AIP content is subject to the terms at: http://scitation.aip.org/termsconditions. Downloaded to IP: 161.111.180.191 On: Wed, 23 Dec 2015 12:43:41